Karadeniz Fen Bilimleri Dergisi
The Black Sea Journal of Sciences
DOI: 10.31466/kfbd.1710641
ISSN (Online): 2564-7377
https://dergipark.org.tr/tr/pub/kfbd

Araştırma Makalesi / Research Article

Design and Performance Comparison of Rotor-Optimized Flux Reversal Machines (FRMs) with Axial and Radial Flux Topologies

Eksenel ve Radyal Akı Topolojilerine Sahip Rotor Optimizasyonlu Akı Tersleyen Makinelerin (ATM) Tasarım ve Performans Karşılaştırması

Harun Serhat GERÇEKCİOĞLU[1]*

Abstract

In this study, the electromagnetic performances of radial-flux and axial-flux Flux Reversal Machines (RF-FRM and AF-FRM) are comparatively investigated following rotor-side geometric optimization. To ensure a fair comparison, the current density in the stator windings is kept identical for both machines, while the stator and stator slot geometries are fixed and excluded from the optimization process. This approach is adopted to ensure that the observed performance differences arise solely from the machine topology and rotor geometry. Three-dimensional finite element analyses are carried out using ANSYS Maxwell, and the rotor geometry is optimized through a genetic algorithm with the primary objective of reducing torque ripple. The electromagnetic performance is evaluated in terms of average torque, torque ripple, output power, total losses, efficiency, and torque density. The results indicate that the AF-FRM delivers higher average torque and output power than the RF-FRM, exhibits lower torque ripple, and achieves nearly twice the torque density. Although the total losses of both machines are at comparable levels, the AF-FRM attains higher efficiency due to its increased mechanical output power. These findings demonstrate that axial-flux topologies offer significant advantages for applications requiring high torque density and efficient current utilization.

Keywords: Axial flux machines, Finite element method, Optimization.

Öz

Bu çalışmada, radyal akılı ve eksenel akılı Akı Terslemeli Makinelerin (RF-FRM ve AF-FRM) rotor tarafı geometrik optimizasyonu sonrası elektromanyetik performansları karşılaştırmalı olarak incelenmiştir. Adil bir karşılaştırma sağlamak amacıyla her iki motor için sargılardaki akım yoğunluğu eşit tutulmuş, stator ve stator oluğu geometrileri sabit kabul edilmiş ve bu bölgelere yönelik herhangi bir optimizasyon uygulanmamıştır. Böylece performans farklarının yalnızca motor topolojisi ve rotor geometrisinden kaynaklanması hedeflenmiştir. Üç boyutlu sonlu eleman analizleri ANSYS Maxwell ortamında gerçekleştirilmiş ve rotor geometrisi genetik algoritma kullanılarak tork dalgalanmasının azaltılması amacıyla optimize edilmiştir. Elektromanyetik performans; ortalama tork, tork dalgalanması, çıkış gücü, toplam kayıplar, verim ve tork yoğunluğu kriterleri üzerinden değerlendirilmiştir. Elde edilen sonuçlar, AF-FRM'nin RF-FRM'ye kıyasla daha yüksek ortalama tork ve çıkış gücü ürettiğini, tork dalgalanmasının daha düşük olduğunu ve tork yoğunluğunun yaklaşık iki katına ulaştığını göstermektedir. Toplam kayıplar her iki motor için benzer seviyelerde gerçekleşmesine rağmen, AF-FRM daha yüksek mekanik çıkış gücü sayesinde daha yüksek verim elde etmiştir. Bu bulgular, eksenel akılı topolojilerin yüksek tork yoğunluğu ve etkin akım kullanımı gerektiren uygulamalarda önemli avantajlar sunduğunu ortaya koymaktadır.

Anahtar Kelimeler: Eksenel akılı makineler, Sonlu elemanlar yöntemi, Optimizasyon.

[1]Tokat Gaziosmanpaşa Üniversitesi, Mühendislik ve Mimarlık Fakültesi, Elektrik Elektronik Mühendisliği, Tokat, Türkiye

***Sorumlu Yazar/Corresponding Author:** harun.gercekcioglu@gop.edu.tr

Geliş/Received: 01.06.2025 **Kabul/Accepted:** 14.04.2026 **Yayın/Published:** 04.06.2026

Gerçekcioğlu, H. S. (2026). Design and Performance Comparison of Rotor-Optimized Flux Reversal Machines (FRMs) with Axial and Radial Flux Topologies. *Karadeniz Fen Bilimleri Dergisi*, 16(2), 781-805. https://doi.org/10.31466/kfbd.1710641

1. Introduction

Enhancing energy efficiency and transitioning to clean energy sources have emerged as critical global priorities. According to the 2024 report of the European Parliament Energy Union, the targeted reductions in greenhouse gas emissions are 55% by 2030, 90% by 2040, and ultimately 100% by 2050 (URL-1). In line with these objectives, significant efforts are being made to enhance energy efficiency in both industrial and transportation sectors. Similarly, in Türkiye, collaborations with organizations such as the European Electricity Association (EUROELECTRIC) have facilitated various initiatives aimed at clean energy and efficiency (URL-2). The Ministry of Energy and Natural Resources has evaluated sectoral energy efficiency in its "Energy Efficiency Strategy 2030" reports, highlighting the dominant share of industry and transportation in total final energy consumption (URL-3). Literature confirms that electric machines account for a substantial share of industrial electricity consumption arises from electric machines, underscoring the importance of improving their efficiency. Moreover, in line with the clean energy vision, the adoption of electric motors in transportation is rapidly increasing, leading to a growing interest in the development of innovative motor designs.

Structurally, electric machines are generally categorized into radial flux (RF) and axial flux (AF) types. Historically, it is known that Faraday's first machine developed in 1831 had an axial flux structure. Likewise, the motor patented by Tesla in 1889 was also a disk-type machine. Although the axial flux geometry attracted attention from motor designers, mechanical challenges—particularly those related to maintaining the air gap—limited its practical application. However, the advent of rare-earth permanent magnets has facilitated the effective use of machines with larger air gaps. Permanent magnet machines are now widely used in industrial applications due to their high torque density, energy efficiency, and power density (Patterson et al., 2009; Martins and Labakhua, 2024).

In this study, two Flux Reversal Machine (FRM) topologies were designed: one with a radial flux (RA) structure and another with an axial flux (AF) structure. Both machines feature surface-mounted permanent magnets (PM) located on the stator teeth and operate at 5.5 kW, 1500 rpm, with a three-phase, four-pole configuration. Prior to comparing their performance, rotor-side geometrical optimizations were conducted to reduce torque ripple. The optimization process was carried out using a Genetic Algorithm (GA). All designs and optimizations were performed in three dimensions (3D) using the ANSYS Maxwell Electromagnetic Suite. While RA-FRM topologies are well-represented in the literature, studies on AF-FRM configurations remain limited (Mirzayess et al., 2005; Zhao et al., 2023).

In this study, the term Flux Reversal Machine (FRM) is consistently used to describe machines operating with stator-mounted permanent magnets and flux reversal behavior. It should be noted that

such machines are also classified as flux-switching permanent magnet machines in parts of the literature. In order to avoid ambiguity, the terminology FRM is adopted throughout this paper.

From a geometrical standpoint, FRMs are characterized by permanent magnets mounted on the stator teeth, facing the air gap. This configuration offers a simpler stator structure compared to other PM machines, where magnets are often embedded between winding slots or located in the stator yoke, as seen in switched flux PM machines or double-salient PM machines. Such configurations may complicate stator assembly and result in reduced slot area or increased machine volume. In FRMs, both distributed and concentrated windings can be utilized depending on design preferences (Wang et al., 1999; Wang et al., 2021; Zhao et al., 2014; Sriwannarat et al., 2021; Seangwong et al., 2021).

Despite the well-documented advantages of flux reversal machines, their axial flux counterparts have not been thoroughly explored in the literature. Most existing studies focus on radial flux configurations due to their well-established manufacturing processes and thermal management strategies. However, axial flux topologies offer potential advantages such as shorter axial length, improved torque density, and better integration possibilities in compact systems—particularly relevant in electric vehicle and aerospace applications. By addressing design and optimization challenges associated with axial flux FRMs, this study aims to fill a significant gap in current research and provide a comparative analysis that highlights the performance benefits of axial flux structures over traditional radial flux configurations.

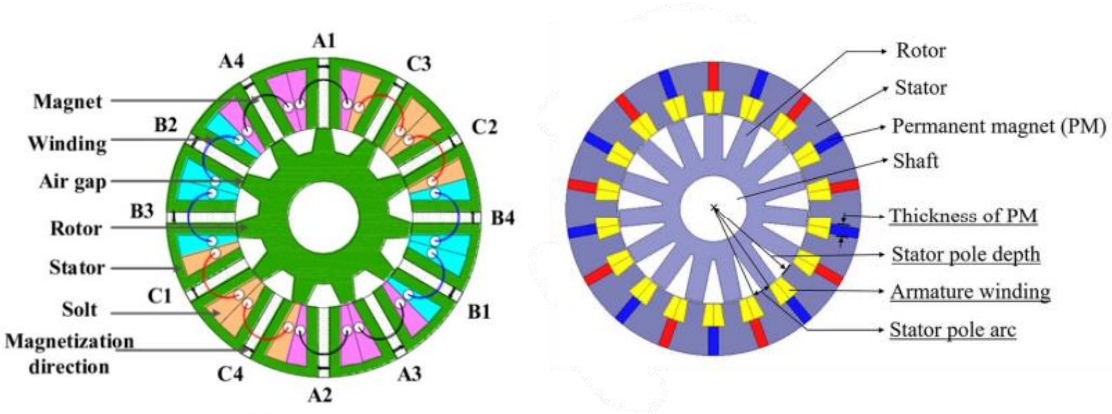

a) b)

Figure 1. (a) Flux-switching permanent magnet machine, (b) doubly-salient permanent magnet machine

From the rotor perspective, there are no rotor windings or permanent magnets (PMs) present. The motor excitation is achieved exclusively through permanent magnets mounted on the stator side, replacing the rotor windings found in DC machines or the squirrel cage structures typical of induction motors (IMs). This unique excitation method significantly reduces rotor copper losses, thereby improving overall machine efficiency and thermal management.

Moreover, the absence of rotor windings simplifies the rotor construction, reducing mechanical stresses and inertia, which can lead to enhanced dynamic performance. The elimination of rotor copper losses also decreases heat generation in the rotor, allowing for more effective cooling strategies focused on the stator.

2. Materials and Methods

The fundamental operating principle of FRMs is illustrated through a representative example utilizing a 2-pole stator and a 3-pole rotor configuration is provided (Deodhart et al., 1997). This example highlights the magnetic flux reversal phenomenon responsible for torque generation, which differentiates FRMs from conventional synchronous and induction machines.

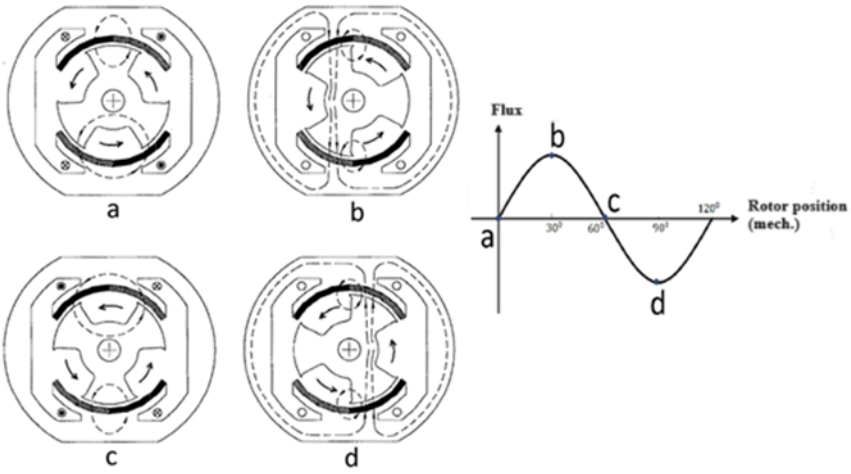

Figure 2. FRM working principle (relationship between flux and rotor mechanical positions))

In Figure 2, position (a) represents the equilibrium state where the magnetic flux produced by the magnets circulates entirely within each stator pole, with no flux present in the stator yoke. At rotor position (b), the rotor has rotated 30° counter clockwise, causing the rotor poles to overlap with one of the magnets. In this position, the flux passes through the windings and the stator yoke, and the phase flux reaches its maximum. When the rotor is at position (c), it reaches a second equilibrium position, having rotated 60° from position (a). At this position, there is again no flux in the stator yoke or in the windings connecting the poles. A further 30° counter clockwise rotation brings the rotor to position (d), where the flux reaches its maximum in the opposite (negative) direction compared to position (b) (Bharathi et al., 2019).

To comprehensively understand the operating principle of the axial flux (AF) design, it is essential to analyze its electromagnetic behavior through the equivalent magnetic circuit model. This model allows detailed examination of flux paths, magnetic reluctance, magnetomotive force (MMF)

distribution, and leakage flux phenomena within the stator and rotor assemblies. Such an approach is critical for accurately predicting performance metrics such as torque production, cogging torque, and efficiency, as well as for guiding the geometric and material optimization of the AF machine.

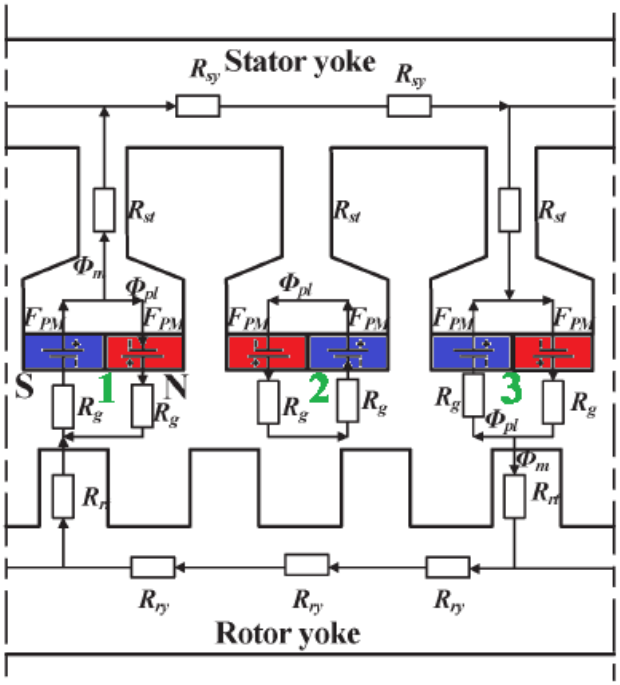

Figure 3. Equivalent Magnetic Circuit of the AF-FRM

In the equivalent magnetic circuit model, the rotor tooth is closer to the S-pole magnet at the stator tooth numbered 1. The S-pole magnet produces two magnetic flux paths: the first is the pole leakage flux, Φ_{pl}, which passes through the adjacent N-pole magnet, and the second is the main flux, Φ_m, which passes through the stator tooth, stator yoke, rotor tooth, and rotor yoke. Thus, the coil flux linkage is established.

At the stator tooth numbered 2, the magnetic field distribution is equidistant from the rotor axis S-pole and N-pole magnets. Therefore, at this moment, the two magnets generate only one magnetic flux path, i.e., the pole leakage flux Φ_{pl}.

At the stator tooth numbered 3, the rotor tooth is closer to the N-pole magnet. The N-pole magnet produces two magnetic flux paths: one is the pole leakage flux Φ_{pl} passing through the adjacent S-pole magnet, and the other is the main flux Φ_m passing through the stator tooth, stator yoke, rotor tooth, and rotor yoke. Thus, the coil flux linkage is established similarly to that at the stator tooth numbered 1. It should be noted that the magnetic flux path at stator tooth 1 is exactly opposite to that at stator tooth 3, and the coil flux polarities in these two states are opposite to each other [Gao and Liu, 2021].

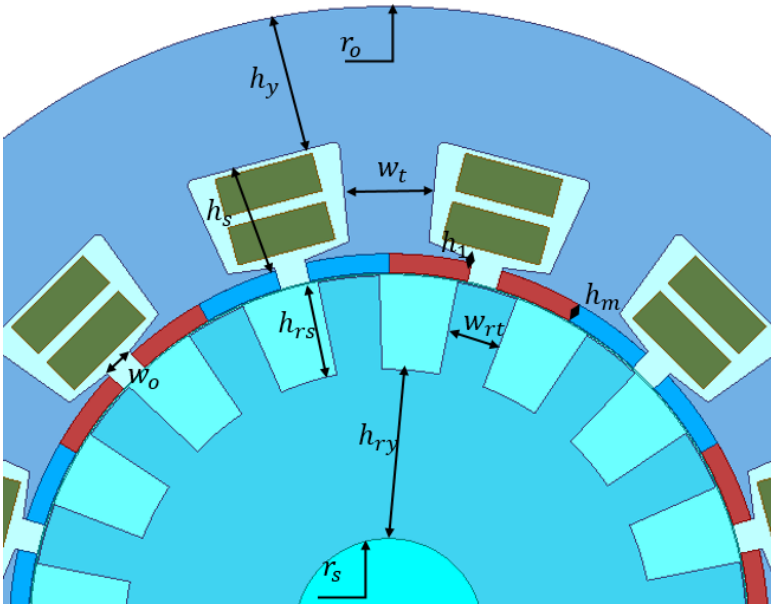

Figure 4. Dimensional parameters of the stator, rotor, and permanent magnets of the RF-FRM

For the selection of stator and rotor pole numbers in the RF-FRM design, the ratio shown in Eq. (1) is employed. Here, N_s represents the number of stator poles, N_r denotes the number of rotor poles, and m is the number of phases:

$$\frac{N_s}{N_r} = \frac{m}{m+1} \tag{1}$$

For the designed FRM, the configurations $N_s/N_r = 3/4, 6/8, 12/16$ are selected. After determining suitable initial design parameters aligned with the motor's intended application, the rotor diameter D_r is calculated. Electromagnetic power P_{eb}, which is related to motor efficiency n_b, is required for determining D_r. The tangential force density defined as f_x, is selected within the range of $1.8 - 2.5\ N/cm^2$ and is used in the electromagnetic power calculation [Boldea et al., 1999; Gao and Liu, 2021] :

$$P_{eb} = \frac{P_b}{n_b} \tag{2}$$

$$P_{eb} = f_x(\pi D_r l)\frac{D_r}{2}\Omega_r = \frac{\pi}{2} f_x \alpha D_r^3 \Omega_r \tag{3}$$

In Eq. (3), α is the ratio between the rotor diameter and axial length, defined as $\alpha = l/D_r$, and can typically be selected within the range of $1.1 - 1.8$.

As a result, D_r can be expressed as:

$$D_r = \left(\frac{2P_{eb}}{\pi f_\chi \alpha \Omega_r}\right)^{1/3} \tag{4}$$

The expression for the electromagnetic torque is presented in Eq. (5).

$$T_{eb} = \frac{P_{eb}}{\Omega_{rb}} \tag{5}$$

Fig. 4 illustrates the stator and rotor geometry of the Flux Reversal Motor (FRM). The equations used to calculate the geometric dimensions depicted in the figure are provided in Eq. (6) through (16), as follows:

$$\phi_m = 2r_g l_{stk} B_m / p \tag{6}$$

Here, r_g denotes the air-gap radius, p represents the number of stator winding pole pairs, B_m is the magnetic flux density, and l_{stk} refers to the active stack length [15, 16]. [Boldea et al., 1999; Gao and Liu, 2021]

If the average flux density in the stator yoke is denoted by B_y the stator yoke thickness h_y can be determined as follows:

$$h_y = \frac{\phi_m}{2B_y k_{stk} l_{stk}} = \frac{r_g B_m}{P B_y k_{stk}} \tag{7}$$

Similarly, if the average flux density at the centre of the stator tooth is denoted by B_t , the stator tooth width can be calculated as follows:

$$w_t = \frac{\phi_m}{3(SPP) B_t k_{stk} l_{stk}} = \frac{4r_g B_m}{Z_s B_t k_{stk}} \tag{8}$$

Here, SPP represents the number of slots per pole per phase, and Z_s denotes the number of stator teeth. To simultaneously maintain a high torque density and minimize the risk of demagnetization of the permanent magnets (PMs), it is recommended that the PM thickness satisfies the condition given in Equation (9).

$$h_m = 4g \sim 6g \tag{9}$$

Here, g represents the air gap length. The stator slot opening width is provided in Equation (10).

$$w_o = \pi(r_g + h_m)/2Z_s \tag{10}$$

To calculate the outer stator radius D_o , it is first necessary to determine the total slot area A_{slot} . In this calculation, the electrical loading A_e , current density j_e , and slot fill factor S_{fg} are utilized [Boldea et al., 2010; Gao and Liu, 2021].

$$A_{slot} = 2\pi\big(r_g + h_m\big)A_e/J_eS_{fg} \tag{11}$$

$$A_{slot} = \pi\big(r_g + h_m + h_1 + h_s\big)^2 - \pi\big(r_g + h_m + h_1\big)^2 - Z_s w_t h_s \tag{12}$$

By combining Equation (11) and Equation (12), the slot depth h_s can be determined. Consequently, the outer stator radius is expressed in Equation (13).

$$r_o = r_g + h_m + h_1 + h_s + h_y \tag{13}$$

The average flux densities at the centre of each rotor yoke and rotor tooth are denoted by B_{ry} and B_{rt}, respectively. The rotor yoke thickness h_{ry} and the rotor tooth width w_{rt} are derived using a procedure analogous to that employed for Equations (7) and (8). Finally, the expressions for h_{ry} and w_{rt} are presented in Equations (14) and (15), respectively.

$$h_{ry} = r_g B_m/Z_r B_{ry} k_{stk} \tag{14}$$

$$w_{rt} = 4r_g B_m/Z_r B_{rt} k_{stk} \tag{15}$$

The rotor slot depth, denoted as h_{rs} , is expressed as follows:

$$h_{rs} = r_s + h_{ry} \tag{16}$$

The dimensional design equations used for the Axial Flux-Flux Reversal Motor (AF-FRM) are derived based on axial flux motor equations. In this approach, the stator and rotor designs are grounded on the standard cylindrical induction and synchronous motor design principles widely accepted worldwide. The obtained parameters are subsequently adapted to the axial flux configuration. Using a fixed magnetic circuit calculation method, the stator and rotor inner and outer diameters, as well as their thicknesses, are adjusted accordingly.

As an example, the structure of a single-stator single-rotor axial flux motor is illustrated in Figure 3. Designs can be implemented in configurations such as double-stator single-rotor or single-stator double-rotor as well. Here, D_o, D_i, g, L_{stator}, L_{rotor} and h_{mag} represent the outer diameter, inner diameter, air gap length, stator stack length, rotor stack length, and magnet length, respectively. The average diameter of the stator, D_{avg}, and the pole pitch, τ_p, are key parameters for torque production [Sahin, 2001; Chlebis et al., 2012].

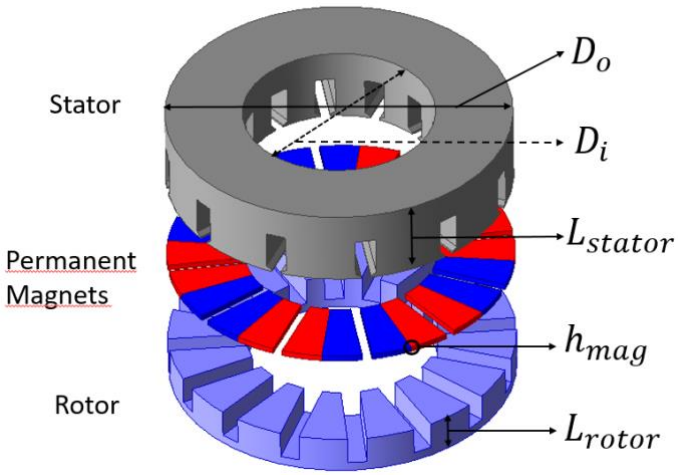

Figure 5. Axial Flux FRM and Dimensional Parameters

$$D_o = \sqrt[3]{\frac{\varepsilon P_{out}}{\pi^2 k_D k_{\omega 1} n_s B_{mg} A_m n cos\varphi}} \tag{17}$$

$$D_i = k_d D_o \tag{18}$$

$$D_{avg} = 0.5(D_o + D_i) \tag{19}$$

$$\tau = \frac{\pi D_{avg}}{2p} \tag{20}$$

$$k_D = \frac{1}{8}(1 + k_d)[1 - (k_d)^2] \quad (21)$$

In the given Equation (21), ε refers to the emf-phase voltage ratio, P_{out} refers to output power, k_D expresses a coefficient related to the D_i/D_o ratio. $k_{\omega 1}$ Indicates the winding factor, $n_s$refers to the rotor speed, B_{mg} refers to the peak value of the magnetic flux density in the air gap, A_m indicates the peak value of the line current density, n is the efficiency, $cos\varphi$ indicates the power factor. k_d is the ratio of the inner diameter of the stator to its outer diameter [Gieras et al., 2008].

Thus, the line current density can be expressed as follows:

$$A_m = \frac{m_1\sqrt{2}I_a N_1}{\pi D_{out}(1+k_d)} \quad (22)$$

The apparent electromagnetic power can be expressed as:

$$S_{elm} = \pi^2 k_D k_{w1} n_s B_{mg} A_m D_{out}^3 \quad (23)$$

The average electromagnetic torque is presented in Equation (24).

$$T_d = \frac{P_{elm}}{2\pi n_s} = \frac{S_{elm}\cos\psi}{2\pi n_s} = \frac{\pi}{2} k_D k_{w1} D_{out}^3 B_{mg} A_m \cos\psi \quad (24)$$

Here, P_{elm} denotes the active electromagnetic power, and ψ represents the phase angle between the stator current II$_a$ and the electromotive force E_f. It can be observed that the torque is proportional to D_{out}^3.

The selection of stator-rotor slots and the number of poles in an Axial Flux Flux Reversal Motor (AF-FRM) is a critical parameter for torque production and average torque density. The choice of the slot-pole combination should aim to maximize the winding factor. In the AF-FRM design, although concentrated windings reduce copper losses, they inherently increase torque ripple. For multiphase FRMs, the number of stator and rotor slots is typically determined using a general rule expressed in Equation (1). [Boldea et al., 2010].

For the three-phase design, a 4-pole configuration with a 12/16 slot-pole combination has been selected. Although this combination and the choice of distributed winding are favorable for achieving high torque, they inherently result in significant torque ripple. In the subsequent sections of this study, torque ripple is mitigated through an optimization process.

The current density J typically ranges between 3 and 7 (A/mm^2). Higher values may be selected if additional cooling equipment is integrated into the machine frame or system. The magnetic flux density B in the magnetic circuits should remain below specific limits, which are determined by the properties of the lamination material used in the machine.

The stator slot fill factor is expressed by the equation $k_{fill} = A_{cu}/A_{su}$, where A_{cu} represents the total copper area and A_{su} denotes the stator slot area. When distributed windings are used, a fill factor of approximately 0,4 - 0,6 is considered acceptable [EL-Refaie, 2010].

This value may vary depending on insulation thickness and conductor geometry. The ratio of the inner diameter to the outer diameter k_d is directly influenced by the number of poles.

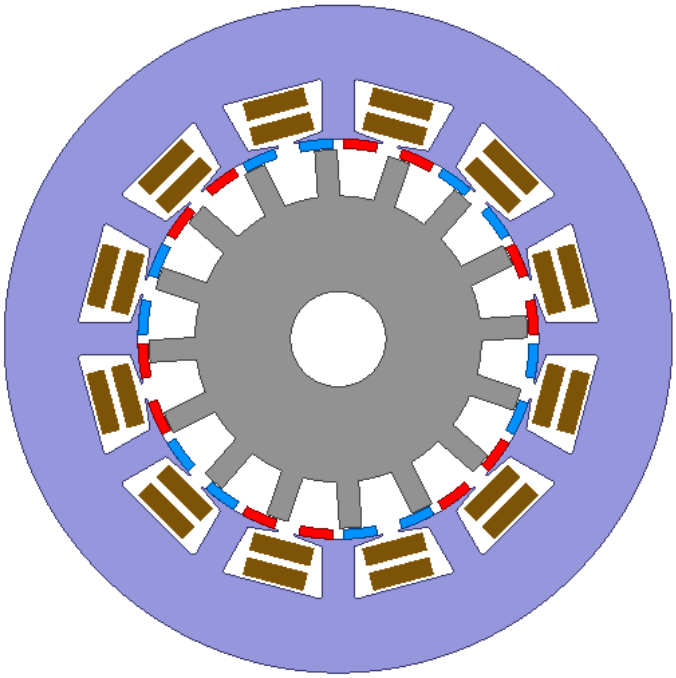

a)

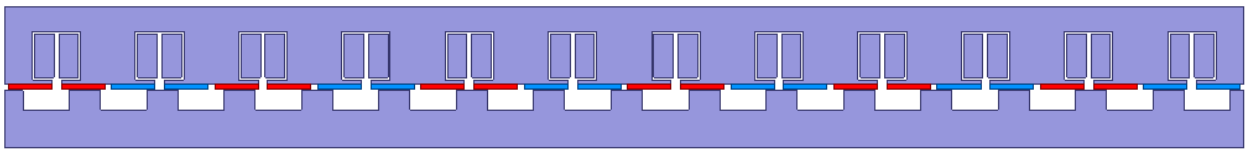

b)

Figure 6. 2D models of a) RF-FRM b) AF-FRM

To enable a fair comparison between both designs, the initial design parameters were selected to be identical. A rated power of 5,5 kW was chosen, representing a medium power level that is commonly used across various application domains. Motors in this power range are widely employed in industrial, agricultural, and commercial sectors. They are commonly used in constant-speed applications such as pumps and fans, as well as in custom-designed electric vehicles like small boats

and golf carts. To reduce the computational cost of electromagnetic analyses, 2D models were created and analyzed for both motor types (Figure 6).

Table 1 presents the initial design parameters for both motors. Table 2 presents material of machine parts. The volumes of the permanent magnets are given in Table 3, and they have been selected to be as equal as possible. The preliminary sizing parameters for the RF-FRM and the AF-FRM are given in Table 4 and Table 5, respectively.

Table 1. Initial parameters for the RF-FRM and AF-FRM designs

Initial Parameters	Description	Value
P_o	Output power	5.5 kW
V	Voltage	380 V
ω	Speed	1500 rpm
g	Air gap	0.5 mm
N_s	Stator slot number	12
N_r	Rotor teeth number	16
η	Efficiency	% 90
h_m	Permanent magnet height	3 mm
$cos\ \varphi$	Power factor	0.7
$B_{mg}A_m$	Magnetic flux-Electric load	26000 TA/m
q_s	Slot number per phase-per pole	3
J	Current density	7 A/mm2
k_{st}	Lamination factor	0.97
k_w	Winding factor	0.97
k_{fill}	Fill factor	0.50
k_d	Stator inner/outer ratio	0.58

Table 2. Material of machines parts

Machine part	Material	Type
Stator	JFE_Steel_50JN1000	Lamination
Rotor	Steel_1010	Solid
Permanent Magnets	NdFeB	Rare-earth

Table 3. Permanent magnets volumes

Machine part	Material	Total Volume
RF-FRM Magnets	NdFeB	91776 mm^3
AF-FRM Magnets	NdFeB	91789 mm^3

To ensure a fair and topology-focused comparison, the current density in the stator windings is set to be identical for both machines. Furthermore, the stator and stator slot geometries are intentionally kept fixed, and no optimization is applied to these components. In this study, only the rotor-side geometric parameters are optimized, allowing the influence of rotor geometry and machine topology on torque ripple and electromagnetic performance to be isolated. It should be noted that additional reductions in torque ripple are expected if stator and slot geometries are also included in the optimization process.

Table 4. Preliminary sizing parameters for the RF-FRM

Parameters	Description	Value
D_o	Stator outer diameter	210 mm
h_y	Stator yoke height	25 mm
h_1	Stator slot entry tooth height	1.5 mm
h_s	Stator slot depth	15 mm
w_o	Stator slot opening width	5 mm
w_t	Stator tooth width	10 mm
Bs_1	Stator slot top width	24.1861 mm
Bs_2	Stator slot bottom width	32.2246 mm
h_m	Permanent magnet thickness	3 mm
D_r	Rotor outer diameter	122 mm
h_{rs}	Rotor tooth depth	14.458 mm
h_{ry}	Rotor yoke height	30 mm
w_{rt}	Rotor tooth width	6.9328 mm
L	Stack length	120 mm
W_1	Number of turns per slot	100
a_1	Number of parallel paths	1
d_{co}	Wire diameter	1 mm
R_s	Stator winding resistance	1.426 ohm
K_{fill}	Stator slot fill factor	% 48.6305

Table 5. Preliminary sizing parameters for the AF-FRM

Parameters	Description	Value
D_o	Stator and Rotor outer diameter	180 mm
D_i	Stator and Rotor inner diameter	105 mm
b_{s0}	Stator Slot openness width	5 mm
b_{s1}	Stator Slot top width	19.7429 mm
b_{s2}	Stator Slot bottom width	19.7429 mm
h_{s0}	Stator Slot openness height	1 mm
h_{s1}	Stator Slot entrance height	1.69796 mm
h_{s2}	Stator Slot height	25 mm
r_s	Stator Slot bottom wrap	1 mm
τ_1	Stator teeth width	22 mm
W_1	Number of conductor per slot	120
d_{co}	Wire diameter	1 mm
a_1	Parallel branches	1
R_s	Stator resistance	1.631 ohm
K_{fill}	Stator slot fill factor	% 49.2996
L_{stator}	Stator length	50 mm
L_{rotor}	Rotor length	30 mm
h_m	Permanent magnet thickness	3 mm

2.1. Parametric Analysis

After completing the initial parameter selection and dimensioning for both models, analyses were conducted to determine the electromagnetic and electrical characteristics of the motors. Finite Element Method (FEM), recognized as a reliable and precise numerical tool for solving complex electromagnetic field problems in electric machines, was utilized for these analyses (Wang et al., 2021; Zhang et al., 2022). The simulations were carried out using the ANSYS Electromagnetics Suite, specifically Maxwell 3D, which subdivides motor components—such as the stator, rotor, magnets, and air gap—into tetrahedral mesh elements to accurately solve Maxwell's equations in three dimensions. Mesh density and quality were iteratively refined to balance between computational efficiency and solution accuracy, as mesh refinement critically affects the precision of the results (Li et al., 2020). Furthermore, the FEM model's reliability was confirmed by cross-validation with both analytical models and experimental results reported in recent literature, reinforcing the accuracy of the simulations for motor design optimization and performance assessment (Chen et al., 2019; Kumar & Singh, 2023). These comprehensive FEM analyses thus establish a robust foundation for the subsequent optimization studies and detailed performance evaluations. (Chen et al., 2019; Li et al., 2020; Wang et al., 2021; Zhang et al., 2022; Kumar and Singh, 2023)

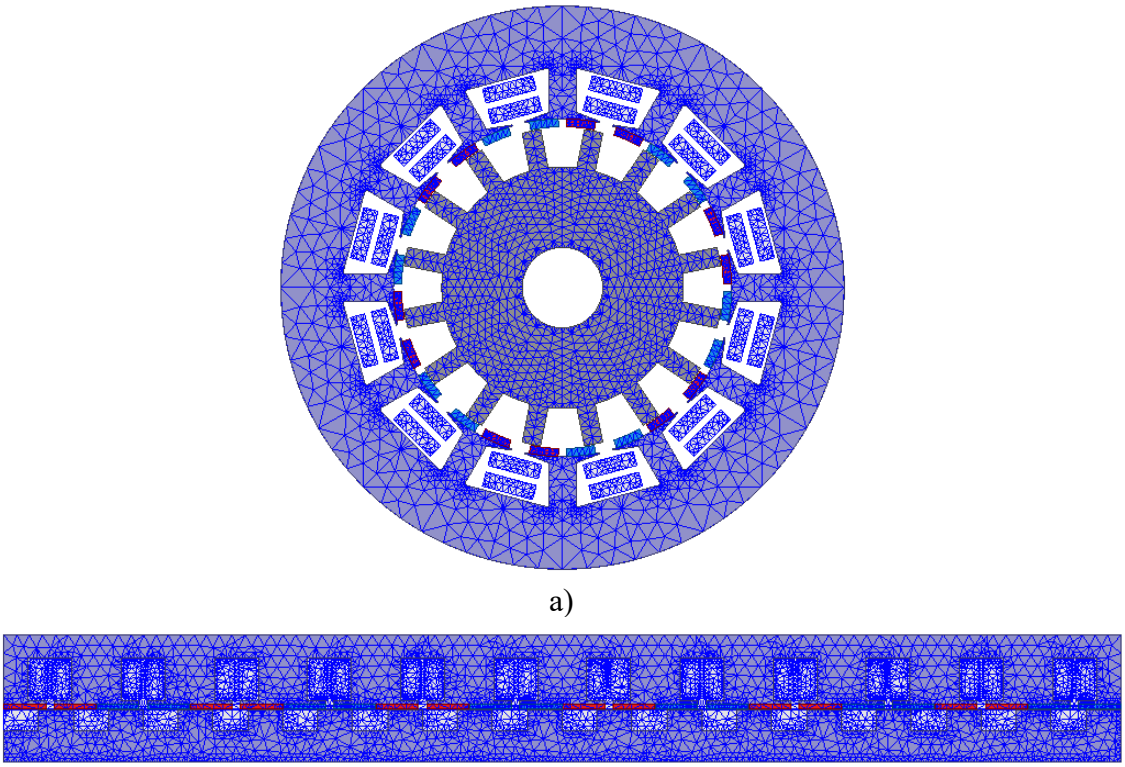

a)

b)

Figure 7. Mesh models of a) RF-FRM b) AF-FRM

Table 6. Mesh Statistics for FEM Models

Model Parts	RF-FRM	AF-FRM
Stator	3849	3740
Rotor	1889	1972
Coils	1632	1748
Regions	5371	5349
Magnets	1287	1314
Total number of elements	14316	14123

In the excitations of the models, a current source was utilized to accelerate the analysis time and to incorporate the maximum torque angle into the excitations. The applied three-phase currents are sinusoidal waveforms and are expressed by the following equations.

Rotor angular velocity Ω_r;

$$\Omega_r = 2\pi\omega/60 \tag{25}$$

$$\Omega_e = \Omega_r \mathrm{N}_r \tag{26}$$

Here, N_r denotes the number of rotor teeth. The applied three-phase currents are expressed as follows:

$$I_A = I_{max}\sin(\Omega_e t + \beta) \quad (27)$$

$$I_B = I_{max}\sin(\Omega_e t + \beta + 120^0) \quad (28)$$

$$I_C = I_{max}\sin(\Omega_e t + \beta - 120^0) \quad (29)$$

Equations (27), (28), and (29) define β as an angular parameter, which is crucial for achieving maximum torque with the applied current. To determine the optimal value of β, angular variations were performed at specific intervals in the AF-FRM model. The angles that yielded maximum torque were identified, and these angle values were incorporated into subsequent current analyses (Table 7). The analyses in this study were conducted with time steps of 0.0001 s over a total duration of 0.04 s.

Table 7. Parametric analysis (β)

	RF-FRM	AF-FRM
Maximum Torque Angle ($\boldsymbol{\beta}$)	90^0	10^0

Since the main objective of the study is to investigate the relative performance of radial- and axial-flux motor topologies with an equal permanent magnet volume, the current density was constrained to 6 A/mm²—an operational and thermal limit considered more conservative for continuous operation—rather than being raised to the upper limits recommended in the literature (≈ 7 A/mm²). Although a detailed thermal design is beyond the scope of this study, previous thermal analyses for J = 6 A/mm² have shown that copper losses and resulting winding temperatures remain at manageable levels under proper cooling (see Du et al. 2022). Under this assumption, the results are evaluated based on electromagnetic performance parameters in order to focus on the comparative analysis of the topologies. To ensure a fair comparison, the maximum phase current was adjusted to achieve equal current density in both machines, resulting in 15 A for the RF-FRM and 14 A for the AF-FRM (Figure 8).

Table 8. Initial performance results

Motor Type	Average Torque (Nm)	Torque ripple (%)	Output Power (Watt)
RF-FRM	32.2001	48.25	5057.9863
AF-FRM	33.8938	44.27	5320.1431

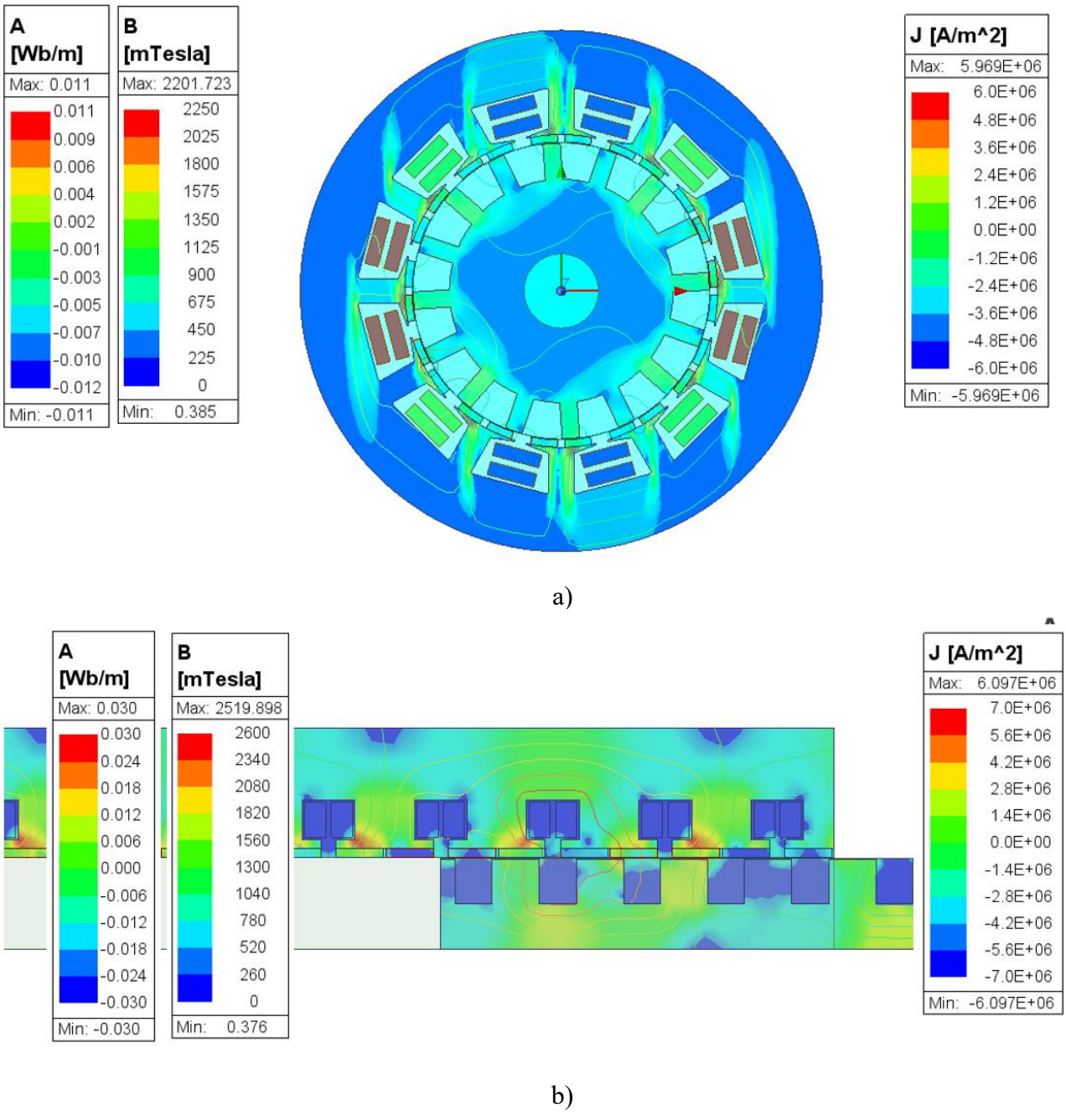

Figure 8. Magnetic vector potential (A)-Magnetic flux density (B) and current density (J) a) RF-FRM b) AF-FRM

After determining the optimal current phase angle (β) that yields the maximum electromagnetic torque through parametric analysis, both the torque characteristics and overall performance of the RF-FRM and AF-FRM were quantitatively evaluated. Table 8 presents the resulting average torque, torque ripple, and output power values for each motor topology. The output power values, which closely align with the rated design target of 5.5 kW, confirm the adequacy of the initial sizing and excitation parameters.

Despite achieving the desired power output, the torque ripple values observed in both configurations indicate significant periodic variations in torque over a single electrical cycle. These

torque ripple components can lead to mechanical vibrations, acoustic noise, and reduced system reliability, particularly in applications requiring smooth and stable torque delivery such as electric vehicles and servo drives**.** The pronounced torque ripple indicates suboptimal initial rotor geometries, although functional, are suboptimal in minimizing harmonic content in the air-gap flux density distribution [Kim et al., 2022; Khan et al., 2021].

Therefore, the analysis underscores the necessity for further design refinement through optimization processes. Advanced optimization techniques—such as Genetic Algorithms (GA) or Multi-Objective Optimization—can be employed to minimize torque ripple while preserving the desired torque and power output **[**Song et al., 2023**].** This may involve adjustments to rotor tooth geometry, magnet placement, or stator slot configuration. The upcoming sections present such an optimization framework, where the objective is to enhance performance indices, particularly reducing torque ripple without compromising the motor's electromagnetic efficiency or structural integrity [Wang et al., 2020; Song et al., 2023].

2.2. Optimization

Genetic Algorithms (GAs) constitute a prominent class of population-based, heuristic direct search methods inspired by the principles of biological evolution. In GAs, individuals representing potential solutions are modeled using chromosome structures, and evolutionary operators such as selection, crossover, and mutation are iteratively applied to generate new generations based on a predefined fitness function. This approach has been proven to be highly effective in solving high-dimensional, nonlinear, and multi-objective optimization problems, providing a robust global search strategy [Holland, 1975; Goldberg, 1989].

In the present study, the genetic algorithm is specifically employed for rotor-side geometric optimization with the primary objective of torque ripple reduction, rather than performing a generic multi-objective optimization over the entire machine geometry.

Rotor design in electrical machines represents a complex engineering challenge that requires the simultaneous optimization of multiple interdisciplinary criteria, including electromagnetic performance, thermal management, structural integrity, and aerodynamics. Traditional deterministic optimization techniques often fall short in such scenarios due to the high nonlinearity of the solution space and the existence of multiple local optima. In this context, the population-based evolutionary nature of GAs offers a distinct advantage by enabling global search capabilities, which result in more reliable and higher-quality optimal solutions [Deb, 2001].

In rotor design, GA implementations are commonly integrated with electromagnetic simulation tools (e.g., ANSYS Maxwell, FEM-based models), which enable accurate performance evaluation of

design parameters in each iteration. This integration facilitates optimization processes based on realistic physical models with high fidelity. Key GA parameters—such as population size, crossover and mutation rates, and the number of iterations—must be carefully chosen according to the specific characteristics of the design problem to balance computational cost and optimization quality. In the present study, high torque ripple values were observed in both motor configurations. To mitigate torque ripple and enhance other performance metrics, optimization was conducted on the rotor side. Incompatibilities between rotor teeth and pole numbers can lead to undesirable harmonic components in the torque profile, resulting in increased torque ripple. Therefore, selecting compatible tooth and pole number combinations is crucial in minimizing torque ripple in motor design [Zhu et al., 2009; Sayyed et al., 2024].

In this study, a torque ripple threshold of 10% was established as the optimization target for the axial flux flux-reversal machine (AF-FRM). This value aligns with the widely accepted standard in the literature, where torque ripple levels below 10% are considered suitable for typical permanent magnet (PM) machines due to their favorable balance between performance, manufacturability, and control complexity. Previous research highlights that maintaining torque ripple under this threshold ensures sufficiently smooth torque output for a broad range of industrial applications. Moreover, reducing torque ripple below 10% has been shown to play a crucial role in minimizing vibration and noise in PM synchronous machines. Consequently, adopting a 10% torque ripple target in the optimization process is both practical and consistent with established electromagnetic design guidelines [Zhu et al., 2009; Jedryczka et al., 2020].

In the optimization study, a target torque ripple level of 10% was defined. Because the magnetic flux density within the windings and the magnet volumes were constrained to remain constant in this comparative framework, the optimization process was intentionally limited to the rotor geometry. In comprehensive structural optimization studies, additional electromagnetic and geometric design variables—such as stator slot widths (slot opening and slot root), stator tooth dimensions, magnet width, and magnet height—are commonly incorporated to broaden the design space and improve solution convergence. The literature indicates that torque-ripple-oriented optimization frameworks can yield substantially lower ripple levels when these expanded parameter sets are included.

However, in order to ensure methodological consistency and maintain a fair basis for comparison across configurations, the present study confines geometric optimization strictly to the rotor side. This constraint isolates the effects of rotor topology on torque ripple behavior and prevents confounding improvements arising from stator-side geometric alterations.

The dimensional parameters modified during the rotor optimization process are illustrated in Figure 9, while the optimized parameter values obtained as a result of the genetic algorithm-based optimization are presented in Table 9.

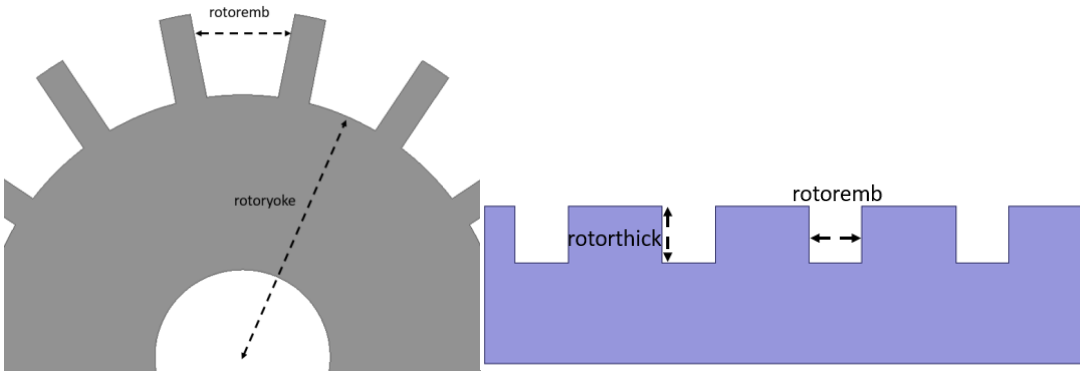

a) b)

Figure 9. Optimization Parameters of RF-FRM (a) and AF-FRM (b)

For the RF-FRM, the selected geometric parameters for rotor-side optimization include rotor teeth wedge, slot body bottom fillet, and rotor yoke height. In the case of the AF-FRM, the optimized parameters comprise slot body height, slot wedge width, slot body bottom width, and slot body bottom fillet. These parameters were systematically varied with the objective of improving torque characteristics and minimizing torque ripple. The optimization results revealed notable enhancements in the electromagnetic performance of both RF-FRM and AF-FRM topologies, thereby demonstrating the effectiveness of the employed optimization methodology.

Table 9. Optimization Ranges and Post-Optimization Values for RF-FRM and AF-FRM

Motor Type	Optimization Parameters	Description	Minimum Value	Maximum Value	Optimized Value
RF-FRM	$rotor_{emb}$	Slot wedge width (mm)	4	16	15.08
	$rotor_{yoke}$	Rotor yoke height (mm)	30	40	30.11
AF-FRM	$rotor_{hs2}$	Slot body height (mm)	5	20	10.32
	$rotor_{emb}$	Slot wedge width (mm)	5	20	10.36

3. Findings and Discussion

This section presents the outcomes and principal findings derived from the conducted study, while also enabling a critical comparison with existing academic and scientific literature relevant to the subject matter.

Within this framework, a comparative evaluation of the electromagnetic performance characteristics of RF-FRM and AF-FRM motor topologies is carried out based on the results obtained before and after the implementation of rotor geometry optimization. The analysis focuses on key performance parameters—namely average torque, torque ripple, and output power—which play a

decisive role in determining overall motor efficiency, torque stability, and applicability in industrial environments.

The results following the optimization process indicate notable performance enhancements for both motor configurations. Nevertheless, the AF-FRM topology exhibits a distinct superiority, particularly with respect to the reduction of torque ripple and the improvement of average torque output. Owing to its distinctive structural arrangement and more effective exploitation of the magnetic flux path, the AF-FRM achieves greater torque density and lower ripple levels while operating at the same power rating. These attributes render the AF-FRM especially advantageous for applications requiring accurate torque regulation and high operational performance.

Moreover, although both motor types deliver comparable levels of output power, the optimized AF-FRM design demonstrates enhanced energy efficiency and diminished electromagnetic losses, thereby offering improved overall operational effectiveness. The findings of this study not only confirm the validity of the genetic algorithm–based optimization strategy for both RF-FRM and AF-FRM configurations, but also provide quantitative support for the superior performance capability of axial flux motor topologies in contemporary electrical machine design.

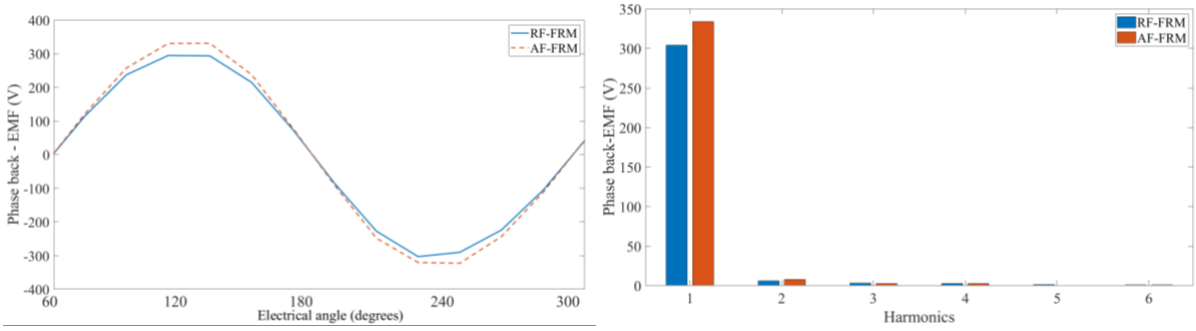

a) b)

Figure 10. Back EMF characteristics (a) Waveform (b) Harmonic spectra

Figure 10 presents a comparative harmonic spectrum analysis of the phase back electromotive force (back-EMF) for the RF-FRM and AF-FRM machine models. It is observed that the AF-FRM model exhibits a higher fundamental component compared to the RF-FRM model, while both models demonstrate comparable harmonic levels. The calculated total harmonic distortion (THD) values are 3.17% for the RF-FRM model and 3.54% for the AF-FRM model. Although a slight increase in THD is observed in the AF-FRM model, the distortion levels for both models remain low and within acceptable limits. These results indicate that the increase in the fundamental back-EMF component in the AF-FRM model is achieved without causing a significant degradation in waveform quality.

Table 10. After optimization performance results

Parameters	RF-FRM	AF-FRM
Average torque (Nm)	33.96	36.12
Torque ripple (%)	16.49	12.17
Output power (W)	5335.02	5671.57
Total loss (W)	1069.57	1072.27
Efficiency (%)	83.3	84.1
Torque density (kN·m/m³)	8.17	16.9

Table 10 presents a comparative performance evaluation of the radial-flux motor (RF-FRM) and the axial-flux motor (AF-FRM operating at the same working conditions. The AF-FRM produces a higher average torque of 36.12 Nm compared to 33.96 Nm for the RF-FRM, which results in an approximately 6.3% increase in output power. In addition, the torque ripple of the AF-FRM is significantly lower (12.17%) than that of the RF-FRM (16.49%), indicating smoother torque production and reduced harmonic content. This characteristic is beneficial in terms of electromagnetic performance and is expected to contribute to lower additional and iron losses.

Since the stator and slot geometries are not optimized in this study, the reported torque ripple values represent the improvement achieved solely through rotor-side optimization

Despite both motors exhibiting comparable total loss levels of approximately 1.07 kW, the AF-FRM achieves a higher overall efficiency of 84.1%, whereas the RF-FRM reaches 83.3%. This efficiency improvement is primarily attributed to the higher mechanical output power delivered by the AF-FRM under similar loss conditions. The most pronounced distinction between the two topologies is observed in torque density. The AF-FRM attains a torque density of 16.9 kN·m/m³, which is more than twice that of the RF-FRM (8.17 kN·m/m³). This outcome highlights the inherent advantage of axial-flux machines in achieving compact designs with high torque capability, owing to their larger effective radius and reduced axial length. Overall, the results demonstrate that the AF-FRM offers a more compact and performance-efficient solution, while the RF-FRM represents a conventional topology with comparatively lower torque density under the same operating constraints. Figure 11 compares the torque–current characteristics of the radial-flux motor (RF-FRM) and the axial-flux motor (AF-FRM). Both machines exhibit an approximately linear torque increase over the investigated current range, indicating operation largely within the linear electromagnetic region. However, for identical current levels, the AF-FRM consistently delivers higher torque than the RF-FRM, demonstrating a superior torque constant. This behavior can be attributed to the more effective utilization of the air-gap radius and electromagnetic shear stress in the axial-flux topology. Furthermore, the reduced current requirement of the AF-FRM for a given torque level implies lower copper losses, which contributes positively to overall efficiency. Although minor saturation effects

are observed at higher currents for both motors, the relative performance advantage of the AF-FRM is maintained across the entire operating range.

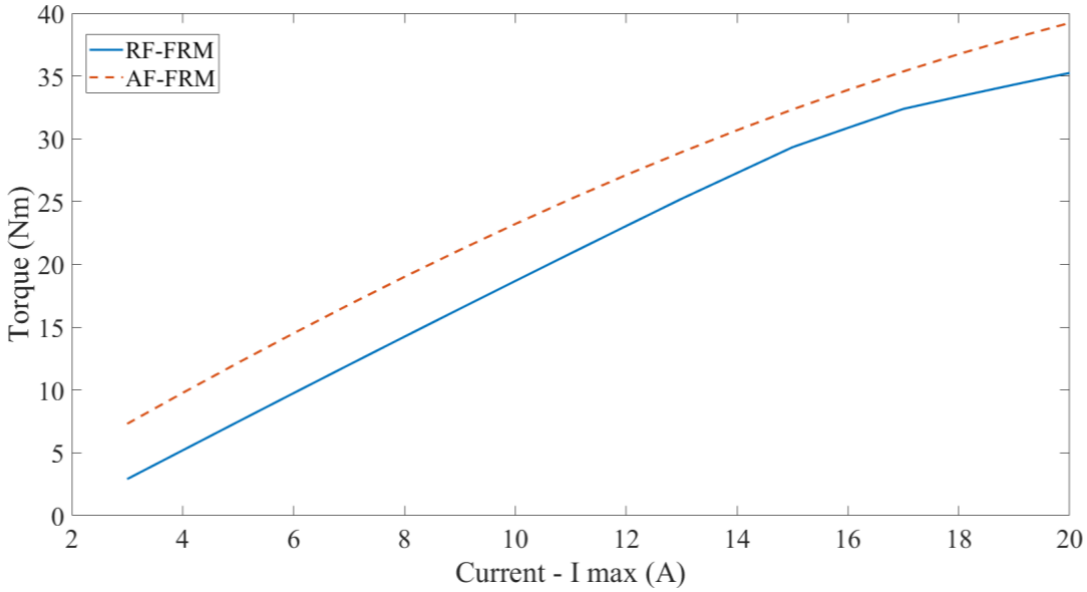

Figure 11. Torque current curves

4. Conclusions and Recommendations

In this study, the performances of radial-flux and axial-flux flux reversal machines designed under identical current density and fixed stator–slot geometry conditions are comparatively evaluated. The effect of rotor-side geometric optimization on both topologies is isolated and examined, demonstrating that this approach is effective in reducing torque ripple. According to the numerical results, the AF-FRM produces an average torque of 36.12 Nm and an output power of 5.67 kW, whereas the RF-FRM delivers 33.96 Nm average torque and 5.34 kW output power. In addition, the torque ripple of the AF-FRM is limited to 12.17%, while a higher value of 16.49% is observed for the RF-FRM.

From a quantitative perspective, the axial-flux topology achieves approximately a 6.3% increase in output power, a 26% reduction in torque ripple, and more than a twofold improvement in torque density compared to the radial-flux topology under identical current density and permanent magnet volume constraints. Although the total losses of both machines are approximately 1.07 kW, the AF-FRM achieves a higher efficiency of 84.1% due to its increased mechanical output power, compared to 83.3% for the RF-FRM. The most pronounced difference is observed in volumetric performance: the torque density of the AF-FRM is calculated as 16.9 kN·m/m³, which is nearly twice that of the RF-FRM (8.17 kN·m/m³). Furthermore, the torque–current characteristics indicate that the AF-FRM possesses a higher torque constant, enabling it to achieve the same torque level with a lower current requirement.

In this work, the stator and stator slot geometries are deliberately excluded from the optimization process. Consequently, the reported results reflect solely the influence of rotor-side optimization. It is anticipated that incorporating stator and slot geometries into the optimization framework would enable further improvements, particularly in terms of torque ripple reduction and efficiency enhancement. Overall, the results demonstrate that axial-flux flux reversal machines offer a more advantageous solution than radial-flux topologies for applications requiring compact structures, high torque density, and efficient current utilization.

Araştırma ve Yayın Etiği Beyanı

Yapılan çalışmada araştırma ve yayın etiğine uyulmuştur.

References

Bharathi, K. S., Kumar, G. P., & Srinivas, S. (2019). Analysis of flux reversal machine using improved magnetic circuit. *Journal of Electrical Engineering & Technology*, 14(4), 1537–1544. https://doi.org/10.1007/s42835-019-00101-1

Boldea, I., Nasar, S. A., & Tutelea, L. (1999). *Electric drives*. CRC Press.

Boldea, I., Tutelea, L., & Parsa, L. (2010). Axial flux PM brushless machines: A review. *IEEE Transactions on Industrial Electronics*, 58(9), 3697–3707. https://doi.org/10.1109/TIE.2010.2043039

Chen, W., Zhao, K., & Wang, T. (2019). Electromagnetic and thermal analysis of high-torque-density axial-flux machines. *IEEE Transactions on Industry Applications*, 55(4), 3950–3959. https://doi.org/10.1109/TIA.2019.2904003

Deb, K. (2001). *Multi-objective optimization using evolutionary algorithms*. Wiley.

Deodhar, R. P., Rahman, M. F., & Lin, H. X. (1997). Magnetic circuit analysis of flux reversal machine. In *Proceedings of the IEEE Industry Applications Society Annual Meeting* (pp. 66–71). IEEE. https://doi.org/10.1109/IAS.1997.643003

Du, G., Zhang, Q., Zhou, Q., Hu, C., & Pu, T. (2022). Comparison of temperature characteristics of outer rotor low-speed PM motors considering magnetic load and current density. *Applied Sciences*, 12(16), 8339. https://doi.org/10.3390/app12168339

El-Refaie, A. M. (2010). Fractional-slot concentrated-windings synchronous permanent magnet machines: Opportunities and challenges. *IEEE Transactions on Industrial Electronics*, 57(1), 107–121. https://doi.org/10.1109/TIE.2009.2030211

Gao, Y., & Liu, X. (2021). Magnetic circuit model for performance prediction of axial flux machines. *IEEE Transactions on Magnetics*, 57(2), 1–9. https://doi.org/10.1109/TMAG.2020.3035022

Gieras, J. F., Wang, R. J., & Kamper, M. J. (2008). *Axial flux permanent magnet brushless machines* (2nd ed.). Springer.

Goldberg, D. E. (1989). *Genetic algorithms in search, optimization, and machine learning*. Addison-Wesley.

Holland, J. H. (1975). *Adaptation in natural and artificial systems*. University of Michigan Press.

Khan, M. A., Ali, R., & Ahmed, S. (2021). Harmonic minimization in high torque ripple permanent magnet machines. *Electric Power Components and Systems*, 49(8), 734–748. https://doi.org/10.1080/15325008.2021.1925479

Kim, D., Kim, Y., & Lee, S. (2022). Design considerations for torque ripple mitigation in electric propulsion motors. *IEEE Transactions on Industry Applications*, 58(2), 2195–2205. https://doi.org/10.1109/TIA.2021.3133198

Martins, J., & Labakhua, T. (2024). Design of a novel electrical machine with full axial and radial magnetic flux excitation. In *2024 International Symposium on Power Electronics, Electrical Drives, Automation and Motion (SPEEDAM)* (pp. 105–110). https://doi.org/10.1109/SPEEDAM61530.2024.10609093

Mirzayee, M., Bahrami, H., Zabihi, A., & Joorabian, M. (2005). A novel flux-reversal axial flux generator for high-speed applications. In *2005 International Conference on Power Electronics and Drives Systems* (pp. 1152–1155). IEEE. https://doi.org/10.1109/PEDS.2005.1619861

Patterson, D., Javidan, M., & Lee, S. (2009). Design and testing of an axial flux permanent magnet motor for electric vehicle propulsion. *SAE International Journal of Engines*, 2(1), 1109–1116. https://doi.org/10.4271/2009-01-2860

Şahin, F. (2001). *Design and development of a high-speed axial-flux permanent machine* (Doctoral dissertation, Eindhoven University of Technology).

Sayyed, M., Ahmad, A., & Husain, M. (2024). Genetic optimization of rotor slot geometry in PM machines. *Journal of Magnetics*, 29(1), 88–95. https://doi.org/10.4283/JMAG.2024.29.1.088

Seangwong, T., Prakotpol, M., & Wongkasemjit, S. (2021). Rotor design enhancement of switched flux machines for low torque ripple. *Energies*, 14(15), 4651. https://doi.org/10.3390/en14154651

Song, H., Zhang, Y., & Wu, C. (2023). Multi-objective design optimization of axial flux machines using hybrid GA-FEM approach. *IEEE Transactions on Magnetics*, 59(5), 1–9. https://doi.org/10.1109/TMAG.2023.3245678

Sriwannarat, C., Seangwong, T., & Chaiyarat, W. (2021). Optimization of permanent magnet shape for torque ripple reduction in flux reversal machines. *Journal of Electrical Engineering & Technology*, 16(2), 673–681. https://doi.org/10.1007/s42835-020-00632-1

URL-1: European Commission. (2024). State of the Energy Union Report 2024. https://energy.ec.europa.eu/publications/state-energy-union-report-2024_en

URL-2: TEİAŞ. (n.d.). Stratejik plan. https://www.teias.gov.tr/stratejik-plan

URL-3: Republic of Türkiye Ministry of Energy and Natural Resources. (n.d.). Energy efficiency 2030 strategy and second national energy efficiency action plan. https://enerji.gov.tr/Media/Dizin/EVCED/tr/EnerjiVerimlili%C4%9Fi/UlusalEnerjiVerimlili%C4%9FiEylemPlan%C4%B1/Belgeler/2UlusalEnerjiVerimlili%C4%9FiEylemPlan%C4%B1.pdf

Wang, J., Atallah, K., & Howe, D. (1999). Design considerations for a flux-reversal permanent magnet machine. *IEEE Transactions on Magnetics*, 35(5), 4279–4281. https://doi.org/10.1109/20.800671

Wang, Y., Liu, H., & Li, J. (2021). Thermal-electromagnetic design of high-performance axial flux PM machines. *IEEE Transactions on Energy Conversion*, 36(3), 1744–1752. https://doi.org/10.1109/TEC.2021.3069023

Wang, X., Zhang, Z., & Li, M. (2020). Genetic algorithm-based torque ripple minimization in axial flux machines. *Electric Power Systems Research*, 185, 106350. https://doi.org/10.1016/j.epsr.2020.106350

Zhang, T., Liu, F., & Huang, Z. (2022). Accurate FEM-based analysis of torque density in axial flux motors. *IEEE Transactions on Industry Applications*, 58(6), 7291–7301. https://doi.org/10.1109/TIA.2022.3207346

Zhao, Y., Chen, Y., & Lin, Z. (2023). A comparative analysis of AF and RF motor topologies using multi-physics simulation. *IEEE Transactions on Magnetics*, 59(4), 1–9. https://doi.org/10.1109/TMAG.2023.3243013

Zhu, Z. Q., & Howe, D. (2009). Electrical machines and drives for electric, hybrid, and fuel cell vehicles. *Proceedings of the IEEE*, 95(4), 746–765. https://doi.org/10.1109/JPROC.2007.911745